Enhanced thermopower in rock-salt SnTe–CdTe from band convergence†

Jun He,[ab] Jingtao Xu,*[b] Guo-Qiang Liu,[b] Hezhu Shao,[b] Xiaojian Tan,[b] Zhu Liu,[b] Jiaqiang Xu,*[a] Haochuan Jiang[b] and Jun Jiang[b]

$SnCd_xTe$ materials were synthesized by the zone-melting method for this thermoelectric performance study. The X-ray diffraction results show that the lattice parameter decreases with increasing x, following Vegard's law of rock-salt structure SnTe and CdTe. Besides, the room temperature Seebeck coefficients of the $SnCd_xTe$ system are enhanced to >60 μV K^{-1}, larger than those of Cd-doped SnTe synthesized by spark plasma sintering. A large power factor of ~25 μW cm^{-1} K^{-1} is achieved in $SnCd_{0.12}Te$ at 820 K, which rivals those of high performance PbTe-based materials. As a result, the highest ZT of ~1.03 at 820 K was achieved for $SnCd_{0.12}Te$.

Introduction

Thermoelectric materials, which can directly generate electrical power from a heat source, draw lots of attention for potential applications in waste heat recovery.[1–3] The conversion efficient is defined by a dimensionless number, the figure merit $ZT = S^2\sigma T/\kappa_{tot}$, where S, σ, T, and κ_{tot} are the Seebeck coefficient, the electrical conductivity, the absolute temperature, and the total thermal conductivity, respectively.

Lead telluride and its alloys are the best thermoelectric materials in the middle/high temperature range, while the element lead causes some concerns about environmental pollution. Recently, lead-free SnTe was expected to become a possible alternative to PbTe, because they have a similar rock-salt structure ($Fm\bar{3}m$) and electronic band structures.[4,5] However, the highest ZT of SnTe was found to be around 0.5, far below the values of ~2.0 for PbTe alloys.[6,7] SnTe possesses too high a hole-carrier concentration (~10^{21} cm^{-3}) due to intrinsic Sn vacancies, resulting in low Seebeck coefficients.[8,9] Besides, SnTe has a smaller band gap (0.18 eV) and larger energy difference (0.35 eV) between the light-hole band at the L point and the heavy-hole band at the Σ point compared to those of PbTe (0.30 eV and 0.17 eV, respectively).[10,11]

Studies have shown that the carrier concentration can be optimized to 10^{19} to 10^{20} cm^{-3} through doping or self-compensation.[12–15] More importantly, recent attempts have been made to modify the valence band structure of SnTe to improve its thermoelectric performance. Zhang *et al.* reported that In doping can form resonance levels in the valence band of SnTe and greatly improve the Seebeck coefficient.[16] Moreover, alloying with Hg, Cd, Mg, Mn, and Ag(I) has been reported to enlarge the band gap and decrease the energy separation between the light-hole band and heavy-hole band, validating effective band convergence.[12,17–24] First principle calculations have shown that Cd and Hg are more efficient in enhancing the Seebeck coefficients though band tuning than Mg and Mn.[25] Nevertheless, the reported low solubility limit (≤3%) of Cd or Hg in SnTe confines further improvement of the thermoelectric performance.

In the previous report where Cd-doped SnTe alloys were synthesized by SPS processing, the lattice parameter increases as the doping concentration increases.[12] CdTe usually forms the zinc-blend-type crystal structure ($F\bar{4}3m$) with a lattice parameter of 6.48 Å.[26,27] Only in some special conditions, such as under high pressures, can CdTe form the rock-salt-type crystal structure ($Fm\bar{3}m$), and the lattice parameter of 5.81 Å is smaller than the 6.314 Å of SnTe.[28,29] According to Vegard's law, the lattice parameter of $Sn_{1-x}Cd_xTe$ should decrease with increasing x. Besides, the smaller Seebeck coefficients of Cd doped SnTe than those of Mg or Mn doped SnTe at room temperature is also not consistent with first principle calculations.[17–23,25] Therefore, Cd substitution in SnTe needs further confirmation for thermoelectric performance optimization.

In this work, we synthesize a series of high quality $SnCd_xTe$ (x = 0–0.15) by the zone-melting method. The structure and thermoelectric properties have been carefully studied. Our results suggest that Cd substitution in Sn sites can significantly enhance the Seebeck coefficient.

Experimental

Samples with nominal compositions of $SnCd_xTe$ (x = 0, 0.01, 0.03, 0.05, 0.07, 0.09, 0.12, and 0.15) were synthesized by mixing

[a]NEST Lab, Department of Chemistry, College of Sciences, Shanghai University, Shanghai 200444, China. E-mail: xujiaqiang@shu.edu.cn

[b]Ningbo Institute of Materials Technology and Engineering, Chinese Academy of Sciences, Ningbo 315201, China. E-mail: xujingtao@nimte.ac.cn

appreciated ratios of high purity starting materials (Sn granule (1–3 mm, 5 N), Te chunk (5 N), Cd granule (5 N)) in quartz ampoules. The ampoules were evacuated to a pressure of $\sim 10^{-2}$ Pa, flame-sealed, and heated to 1123 K in a rocking furnace. The alloys were then grown in a zone melting furnace at 1123 K with a growth speed of 25 mm h^{-1}. The samples were cut into 10 × 2 × 2 mm^3 bars and Φ 10 × 2 mm^2 plates to measure their thermoelectric properties. Only the middle of the ingots were cut for measurements of thermoelectric performance.

X-ray diffraction (XRD) analysis was conducted in reflection geometry on a Bruker AXS diffractometer. The microstructures were investigated by scanning electron microscopy (JEOL 2100HR) and high resolution transmission electron microscopy (TF20). Energy dispersive X-ray spectroscopy (EDXS) was performed with the Si (Li) detector of an EDAX system (Gemsis Software V 4.61) to confirm the homogeneous composition of the samples.

The Seebeck coefficient and electrical conductivity were measured on an Ulvac Japan ZEM-3 instrument under a low pressure helium atmosphere from room temperature to 820 K. The uncertainty of the Seebeck and electrical conductivity measurements is 5%. The thermal conductivity was calculated from the values of the thermal diffusivity (λ), the density (ρ), and the specific heat capacity (C_p) by the relationship $\kappa_{tot} = \lambda\rho C_p$, where λ was measured using the laser flash diffusivity method in a Netzsch LFA-457 in the range from 300 K to 820 K, see Fig. S1 (ESI),†ρ was determined using the Archimedes principle (Table S1, ESI†), and C_p was calculated based on the previous report.[14] The uncertainty of the thermal conductivity was estimated to be within 10%. The effective carrier concentration (n) was estimated using the relationship $n = 1/(eR_H)$, where e is the elemental charge, R_H is the Hall coefficient that was measured by a physical properties measurement system (Quantum Design, PPMS-9) in magnetic fields ranging from 0 to 5 T. The Hall mobility (μ) was calculated using the relationship $\mu = \sigma R_H$.

Results and discussions

All $SnCd_xTe$ (x = 0, 0.01, 0.03, 0.05, 0.07, 0.09, 0.12, and 0.15) alloys crystallize in the rock-salt type structure (space group no. 225, $Fm\bar{3}m$), as shown in Fig. 1a. No second phase is observed within the detection limit of XRD. The lattice parameters were calculated according to the reflection peak positions and plotted in Fig. 1b. Different from the previous report,[12] the lattice parameter decreases with increasing Cd content. The dashed line in Fig. 1b demonstrates Vegard's law of rock-salt type SnTe (6.314 Å) and CdTe (5.81 Å).[26,27,29,30] For $x \leq 0.03$, the lattice parameter follows Vegard's law, suggesting Cd substitution on Sn sites. From $x = 0.05$, the lattice parameter starts to deviate from Vegard's law, and shows less deviation for $x \geq 0.07$. The smallest lattice parameter of ~6.29 Å suggests a solution limit of 4% Cd in SnTe according to Vegard's law, which is consistent with previous studies.[31] The EDXS results also confirm the Cd amount in SnTe (Table S2, ESI†).

The temperature dependence of electrical conductivity for all samples is shown in Fig. 2a. For each sample, the electrical conductivity decreases with increasing temperature from 300 K

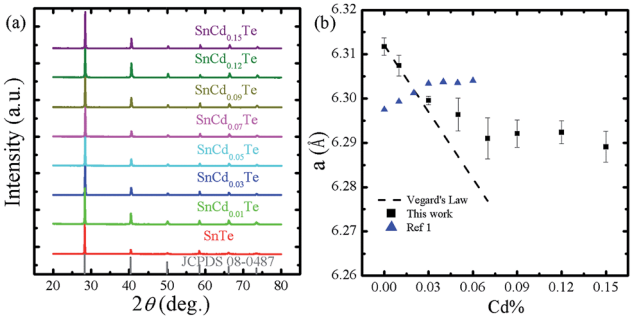

Fig. 1 (a) XRD patterns for $SnCd_xTe$ samples; (b) lattice parameters.

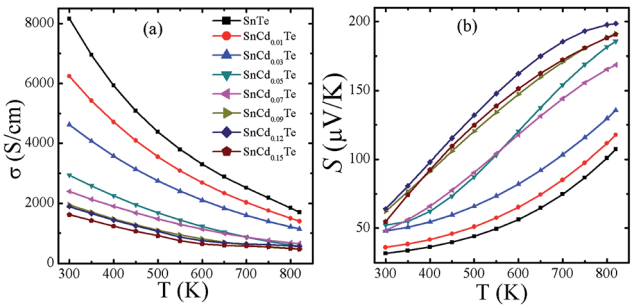

Fig. 2 Temperature dependence of electrical performance for $SnCd_xTe$: (a) electrical conductivity; (b) Seebeck coefficient.

to 820 K. The electrical conductivity gradually decreases with increasing Cd amount. At room temperature, the electrical conductivity decreases from ~8150 S cm^{-1} for pristine SnTe to ~1600 S cm^{-1} for $x = 0.15$. It should be noted that the decrease rate is smaller than in the previous report, in which the electrical conductivity show smaller changes for $x > 0.02$.[12] For the same Cd content of 0.03, the electrical conductivity of our sample was ~4600 S cm^{-1} at room temperature and 1150 S cm^{-1} at 820 K, compared to ~2700 S cm^{-1} and ~500 S cm^{-1} in the previous report.[12]

The Seebeck coefficients as a function of temperature are exhibited in Fig. 2b. The Seebeck coefficients gradually improve with the Cd amount until $x = 0.12$, and then decrease slightly for $x = 0.15$. It is slightly different from the previous report where the Seebeck coefficients for Cd-doped SnTe samples by SPS processing are almost the same for $x > 0.02$.[12] Moreover, for $x > 0.03$ the slope in the S *vs.* T plot decreases with increasing temperature. Similar phenomena have been observed in Hg-doped and Mn-doped SnTe.[17,22] For $x = 0.12$, the Seebeck coefficient nearly saturates at 820 K. The highest Seebeck coefficient of ~200 μV K^{-1} at 820 K in our sample is consistent with in the value obtained from the Cd-doped SnTe by SPS processing.[12]

Previous studies have shown that alloying Hg, Cd, Mn, or Mg with SnTe can validate the effective band convergence and enhances thermoelectric performance.[17–19] First principle calculations have shown that 3% Cd in SnTe can enlarge the band gap to 0.21 eV and reduce the energy difference between the two valence bands to 0.067 eV.[25] While the same amount of Mg and Mn can only reduce the energy difference to 0.13 eV.[25]

Such a trend indicates Cd-doping is more efficient than Mn- or Mg-doping to achieve high Seebeck coefficients.

The room temperature Seebeck coefficients of $SnCd_xTe$ samples were plotted as a function of carrier concentration in Fig. 3. The previous data for Cd-alloyed, Mn-alloyed, and Mg-alloyed SnTe and the theoretical Pisarenko curve are also plotted for comparison.[10,16–18,21] The Seebeck coefficients of all alloyed SnTe are above the Pisarenko curve. When the carrier concentration is in the range of 2 to 3 $\times$ 10^{20} cm^{-3}, the Cd-doped SnTe from SPS processing shows smaller Seebeck coefficients than Mg-doped and Mn-doped SnTe. It can be seen that our results are above the data of Mg-doped and Mn-doped SnTe, which is consistent with the results of first principle calculations. The Seebeck coefficient of 62 $\mu V\ K^{-1}$ at room temperature for $SnCd_{0.12}Te$ is comparable with Hg-doped and In-doped SnTe.[16,17]

The temperature dependence of power factors for the $SnCd_xTe$ samples is plotted in Fig. 4a. Compared to the pristine SnTe, the power factors of Cd-doped samples are greatly enhanced in the temperature range from 400 K to 750 K, due to the improved Seebeck coefficients. The highest power factor was found to be ~25 $\mu W\ cm^{-1}\ K^{-2}$ at 820 K in $SnCd_{0.12}Te$, which is larger than that (~20 $\mu W\ cm^{-1}\ K^{-2}$) of the reported Cd-doped SnTe and rivals those of high performance PbTe-based materials.[32,33]

The total thermal conductivity for the $SnCd_xTe$ system shows a significant decreasing tendency with increasing Cd fraction (Fig. 4b). The room temperature thermal conductivity decreases from 8.6 W $m^{-1}\ K^{-1}$ for pristine SnTe to 3.1 W $m^{-1}\ K^{-1}$ for $SnCd_{0.12}Te$, and then increases a little for $SnCd_{0.15}Te$. The lowest thermal conductivity of ~1.9 W $m^{-1}\ K^{-1}$ was found in $SnCd_{0.12}Te$ above 600 K. The lattice thermal conductivity κ_{lat} was calculated by subtracting the electrical thermal conductivity κ_{ele} from the total thermal conductivity. The electrical thermal conductivity was calculated using the Wiedemann–Franz relationship $\kappa_{ele} = L\sigma T$, where L is the Lorenz number. Lorenz numbers are obtained by fitting the Seebeck coefficient to the reduced chemical potential.[34–36] see Fig. S1 (ESI†). The lattice thermal conductivity for $SnCd_xTe$ samples are plotted in Fig. 4c. Even though some doped samples show lower lattice thermal conductivity than pristine SnTe, there is no accurately definitive dependence between κ_{lat} and x. The modification of total thermal conductivity is mainly due to the control of electrical conductivity. Similar phenomena have been found in doped SnTe alloys.[15,20] The lowest lattice thermal conductivity stays around 1.0 W $m^{-1}\ K^{-1}$. Such a value is still very high compared to high performance PbTe alloys,[32,33] and is also higher than one (~0.7 W $m^{-1}\ K^{-1}$) of the alloys from SPS processing. Normally, the reduction of the lattice thermal conductivity results from strong phonon scattering caused by point defects, dislocations, grain boundaries, and so on. Here, the TEM shows that some dislocations exist in the $SnCd_xTe$ samples and no second phase is observed (Fig. S3, ESI†), suggesting that only dislocations and point defects contribute to additional phonon scattering. Further optimization in the lattice thermal conductivity is expected to achieve better thermoelectric performance.

The ZT values as a function of temperature are plotted in Fig. 4d. After doping Cd, the ZT values are enhanced greatly. Compared to pure SnTe, the highest ZT at 820 K is enhanced ~0.45 to ~0.9 for $SnCd_{0.09}Te$ and further to 1.03 for $SnCd_{0.12}Te$. The highest ZT of 1.03 in the $SnCd_xTe$ samples synthesized by zone-melting is not a great improvement compared to that of 0.96 in samples by SPS processing. One probable reason is the higher lattice thermal conductivity. Higher ZT values can be expected by further decreasing κ_{lat} *via* nanocomposites or alloys.

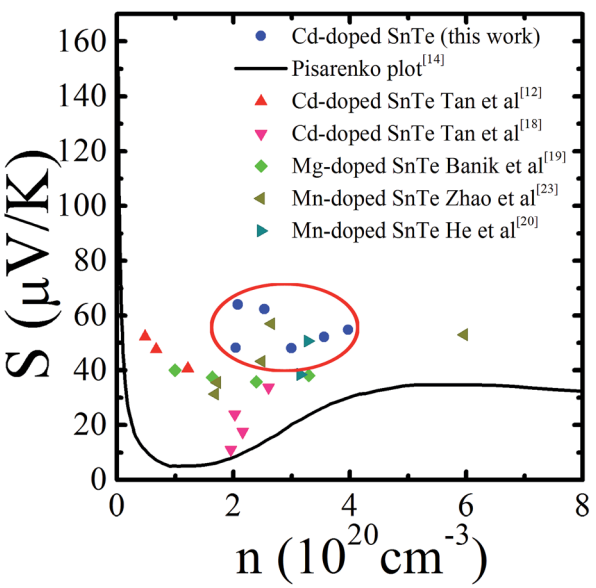

Fig. 3 Room temperature Seebeck coefficient as a function of carrier concentration (n). The line is a theoretical prediction of the S–n relationship based on a VBM model.

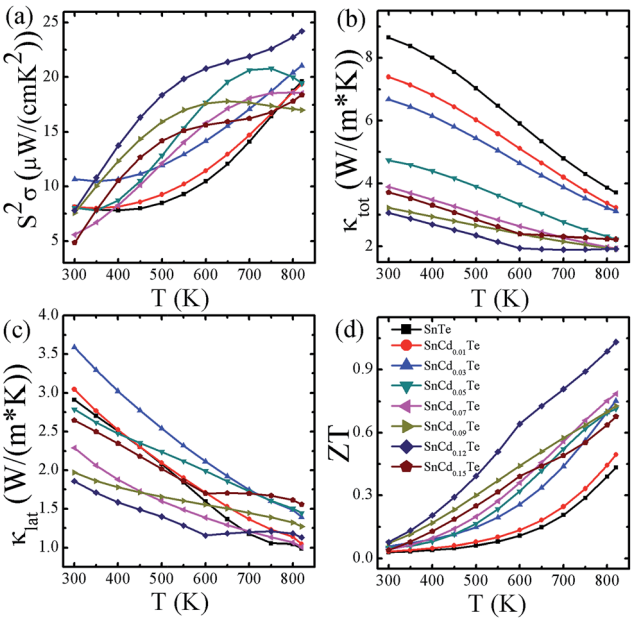

Fig. 4 Temperature dependence for SnTe with different Cd content of: (a) power factor, (b) total thermal conductivity, (c) lattice thermal conductivity, and (d) ZTs.

Conclusions

We synthesized a series of high quality materials of $SnCd_xTe$ by the zone-melting method. The lattice parameter of $SnCd_xTe$ decreases with increasing x, suggesting Cd substitution in Sn sites. The electrical and thermal conductivity decrease with increasing x, and the Seebeck coefficients are greatly enhanced. At room temperature, the Seebeck coefficients of Cd-doped SnTe samples by zone-melting are larger than those of Mg-doped and Mn-doped SnTe, consistent with first principle calculations. A high power factor of $\sim$25 μW cm K^{-2} at 820 K was achieved in $SnCd_{0.12}Te$. As a result, the highest ZT of 1.03 was obtained for $SnCd_{0.12}Te$ at 820 K.

Acknowledgements

This study was supported by the National Nature Science Foundation of China (No. 11304327, 11404348, 11404350, and 11234012), the Ningbo Municipal Natural Science Foundation (No. 2014A610011), the Ningbo Science and Technology Innovation Team (No. 2015A610031, 2014B82004), and Zhejiang Provincial Science Fund for Distinguished Young Scholars (LR16E020001).

References

1 H. J. Goldsmid, *Thermoelectric refrigeration*, 1964.
2 L. E. Bell, *Science*, 2008, **321**, 1457–1461.
3 J. R. Sootsman, D. Y. Chung and M. G. Kanatzidis, *Angew. Chem., Int. Ed.*, 2009, **48**, 8616–8639.
4 P. B. Littlewood, *J. Phys. C: Solid State Phys.*, 1980, **13**, 4855.
5 S. Santhanam and A. K. Chaudhuri, *Mater. Res. Bull.*, 1981, **16**, 911–917.
6 Y. Pei, X. Shi, A. LaLonde, H. Wang, L. Chen and G. J. Snyder, *Nature*, 2011, **473**, 66–69.
7 H. J. Wu, L. D. Zhao, F. S. Zheng, D. Wu, Y. L. Pei, X. Tong, M. G. Kanatzidis and J. Q. He, *Nat. Commun.*, 2014, **5**, 4515.
8 R. F. Brebrick, *J. Phys. Chem. Solids*, 1963, **24**, 27–36.
9 J. A. Kafalas, R. F. Brebrick and A. J. Strauss, *Appl. Phys. Lett.*, 1964, **4**, 93–94.
10 S. Rabii, *Phys. Rev.*, 1969, **182**, 821.
11 R. F. Brebrick and A. J. Strauss, *Phys. Rev.*, 1963, **131**, 104–110.
12 G. Tan, L.-D. Zhao, F. Shi, J. W. Doak, S.-H. Lo, H. Sun, C. Wolverton, V. P. Dravid, C. Uher and M. G. Kanatzidis, *J. Am. Chem. Soc.*, 2014, **136**, 7006–7017.
13 A. Banik and K. Biswas, *J. Mater. Chem. A*, 2014, **2**, 9620–9625.
14 M. Zhou, Z. M. Gibbs, H. Wang, Y. Han, C. Xin, L. Li and G. J. Snyder, *Phys. Chem. Chem. Phys.*, 2014, **16**, 20741–20748.
15 J. He, J. Xu, G. Liu, X. Tan, H. Shao, Z. Liu, J. Xu, J. Jiang and H. Jiang, *RSC Adv.*, 2015, **5**, 59379–59383.
16 Q. Zhang, B. Liao, Y. Lan, K. Lukas, W. Liu, K. Esfarjani, C. Opeil, D. Broido, G. Chen and Z. Ren, *Proc. Natl. Acad. Sci. U. S. A., Early Ed.*, 2013, **110**, 13261–13266.
17 G. Tan, F. Shi, J. W. Doak, H. Sun, L.-D. Zhao, P. Wang, C. Uher, C. Wolverton, V. P. Dravid and M. G. Kanatzidis, *Energy Environ. Sci.*, 2015, **8**, 267–277.
18 G. Tan, F. Shi, S. Hao, H. Chi, L.-D. Zhao, C. Uher, C. Wolverton, V. P. Dravid and M. G. Kanatzidis, *J. Am. Chem. Soc.*, 2015, **137**, 5100–5112.
19 A. Banik, U. S. Shenoy, S. Anand, U. V. Waghmare and K. Biswas, *Chem. Mater.*, 2015, **27**, 581–587.
20 J. He, X. Tan, J. Xu, G.-Q. Liu, H. Shao, Y. Fu, X. Wang, Z. Liu, J. Xu, H. Jiang and J. Jiang, *J. Mater. Chem. A*, 2015, **3**, 19974–19979.
21 W. Li, Z. Chen, S. Lin, Y. Chang, B. Ge, Y. Chen and Y. Pei, *J. Materiomics*, 2015, **1**, 307–315.
22 G. Tan, F. Shi, S. Hao, H. Chi, T. P. Bailey, L.-D. Zhao, C. Uher, C. Wolverton, V. P. Dravid and M. G. Kanatzidis, *J. Am. Chem. Soc.*, 2015, **137**, 11507–11516.
23 H. Wu, C. Chang, D. Feng, Y. Xiao, X. Zhang, Y. Pei, L. Zheng, D. Wu, S. Gong and Y. Chen, *Energy Environ. Sci.*, 2015, **8**, 3298–3312.
24 A. Banik and K. Biswas, *J. Solid State Chem.*, 2016, DOI: 10.1016/j.jssc.2016.02.012.
25 X. J. Tan, H. Z. Shao, J. He, G. Q. Liu, J. T. Xu, J. Jiang and H. C. Jiang, *Phys. Chem. Chem. Phys.*, 2016, **18**, 7141–7147.
26 Y. Sternberg, N. Yellin, S. Cohen and L. B. Dor, *J. Solid State Chem.*, 1982, **43**, 364–367.
27 T. S. Yeoh, S. G. Teoh and H. K. Fun, *J. Phys. Soc. Jpn.*, 1988, **57**, 3820–3823.
28 N. B. Owen, P. L. Smith, J. E. Martin and A. J. Wright, *J. Phys. Chem. Solids*, 1963, **24**, 1519–1520.
29 I. Y. Borg and D. K. Smith, *J. Phys. Chem. Solids*, 1967, **28**, 49–53.
30 A. N. Mariano and E. P. Warekois, *Science*, 1963, **142**, 672–673.
31 E. I. Rogacheva and O. N. Nashchekina, *Phys. Status Solidi A*, 2006, **203**, 2856–2860.
32 K. Biswas, J. He, I. D. Blum, C.-I. Wu, T. P. Hogan, D. N. Seidman, V. P. Dravid and M. G. Kanatzidis, *Nature*, 2012, **489**, 414–418.
33 L. D. Zhao, H. J. Wu, S. Q. Hao, C. I. Wu, X. Y. Zhou, K. Biswas, J. Q. He, T. P. Hogan, C. Uher, C. Wolverton, V. P. Dravid and M. G. Kanatzidis, *Energy Environ. Sci.*, 2013, **6**, 3346–3355.
34 S. Johnsen, J. He, J. Androulakis, V. P. Dravid, I. Todorov, D. Y. Chung and M. G. Kanatzidis, *J. Am. Chem. Soc.*, 2011, **133**, 3460–3470.
35 A. F. May, J.-P. Fleurial and G. J. Snyder, *Phys. Rev. B: Condens. Matter Mater. Phys.*, 2008, **78**, 125205.
36 S. N. Girard, J. He, X. Zhou, D. Shoemaker, C. M. Jaworski, C. Uher, V. P. Dravid, J. P. Heremans and M. G. Kanatzidis, *J. Am. Chem. Soc.*, 2011, **133**, 16588–16597.